Annals of Medicine Research and Public Health
Research Article (ISSN: 2995-5955)

A Dynamical-Systems Formulation of CO_2 Scrubbing in Closed-Circuit Rebreathers

A one-dimensional reaction–diffusion–advection model for different geometry canisters

Sergio Rhein Schirato

Institute of Biosciences, University of Sao Paulo, Brazil

Citation: *Sergio Rhein Schirato. A Dynamical-Systems Formulation of CO_2 Scrubbing in Closed-Circuit Rebreathers. A one-dimensional reaction–diffusion–advection model for different geometry canisters. Ann Med Res Pub Health. 2026;5(2):1-25.*

Received Date: 06 November, 2026; **Accepted Date:** 10 November, 2026; **Published Date:** 11 November, 2026

***Corresponding author:** Sergio Rhein Schirato, Institute of Biosciences, University of Sao Paulo, Brazil.

Copyright: © Sergio Rhein Schirato, Open Access 2026. This article, published in Ann Med Res Pub Health (AMRPH) (Attribution 4.0 International), as described by http://creativecommons.org/licenses/by/4.0/

1. ABSTRACT

The absorption of metabolic carbon dioxide by a packed bed of soda lime absorbent in a closed-circuit rebreather is formulated as a finite-dimensional, non-autonomous dynamical system. Six coupled fields — gas-phase CO_2 and water vapor, gas and solid temperatures, solid CO_2 loading and solid moisture — evolve along a one-dimensional flow path through the canister. Semi-discretization in space by the method of lines maps the governing partial-differential system onto an ordinary differential equation $\dot{y} = F(y,t)$ on $\mathbb{R}^{6N}$, whose vector field is parameterized by canister geometry, absorbent kinetics, a thermal boundary condition and a time-dependent dive profile. Two canisters are treated within one model: an axial bed of circular cross-section (Shape 1) and an axial bed of stadium (rounded-rectangle) cross-section (Shape 2). Both share the same absorbent grade and the same thermal architecture: each cartridge sits inside a larger outer canister, and scrubbed gas returns up the annular jacket, so the bed wall faces warm returning gas rather than cold water. It is shown that geometry enters the vector field only through the cross-sectional area $A(x)$ and the specific wall area $\sigma(x)$, and the jacket only through a scalar recovery factor r attenuating the wall coupling. A steady-state energy balance is then used to bound r: because the reaction liberates of the order of 80 W and the wall is the principal heat sink in the model, only modest values ($r \approx 0.1$–0.3) yield physical bed temperatures (at the nominal wall coefficient; only $(1-r)h_w$ is identifiable), whereas large r drives the bed to unphysical temperatures. Capacity and breakthrough duration are computed as outputs — utilization is not prescribed but emerges from Monte Carlo initiation and passivation of reactive domains within the bed — and breakthrough is defined as the first-hitting time of a scalar observable. In an ensemble of 40 Monte Carlo realizations per canister (EN 14143 baseline: 100 m, 4 °C water, 20 breaths min^{-1} of 2.0 L, CO_2 1.6 L min^{-1}), breakthrough occurred at 155 ± 4 min for Shape 1 and 143 ± 4 min for Shape 2, with emergent utilizations of 0.66 and 0.65, so that most of the difference in duration reflected the difference in absorbent charge.

Keywords: Closed-circuit rebreather; Soda lime; CO_2 Absorption; Packed bed; Reaction–diffusion–advection; Breakthrough time; Non-autonomous dynamical system; Monte Carlo simulation

2. INTRODUCTION AND SCOPE

In a closed-circuit rebreather (CCR) the diver rebreathes the same gas, and the carbon dioxide produced by metabolism must be removed chemically rather than vented. The loop gas is passed through a canister packed with granular soda lime, in which CO_2 is captured by hydroxide bases in an exothermic, water-mediated reaction. The canister has finite capacity: the absorbent saturates progressively from the inlet, and once the reactive zone reaches the outlet, CO_2 reappears in the inhaled gas. The time at which this occurs — the breakthrough time — is the quantity of practical interest, and it depends on absorbent mass, canister geometry, gas flow, metabolic load, ambient pressure and, notoriously, water temperature. One of the most comprehensive studies published on the subject was produced by the Navy Experimental Diving Unit [1, 2] , although many other studies evaluated different aspects of scrubber duration [3, 4] .

The aim here is methodological rather than predictive. It was set out how the scrubber is written as a dynamical system, what the state space is, which structural properties the discretization must preserve, how the canister enters the vector field, and how a safety-relevant threshold event is expressed in that language. The utilization of the absorbent, which is often imposed as a derating factor, is here generated by a stochastic (Monte Carlo) description of the initiation and passivation of the reaction in individual reactive domains of the bed. Although the formulation is deliberately geometry-agnostic, the model was applied to different scrubber geometries, herein denominated Shape one and Shape2. The two canisters are: an axial bed of circular cross-section (Shape 1), and an axial bed of stadium (rounded-rectangle) cross-section (Shape 2). Shape 1 is usually found in back-mount rebreathers, where the scrubber is located on the back of the diver, between the diluent (and / or bail-out tanks), while Shape 2 is usually found in chest-mount units, where the rebreather is located on the chest of the divers, while diluent tanks can be placed in many different configurations.

3. THE PHYSICAL SYSTEM

Exhaled gas enters the canister saturated with water vapor at approximately body temperature, carrying the diver's metabolic CO_2. Within the bed, the dominant chemistry for a calcium-hydroxide absorbent catalyzed by sodium and potassium hydroxide is summarized by the net reaction

$$\mathrm{Ca(OH)_2\,(s) + CO_2\,(g) \rightarrow CaCO_3\,(s) + H_2O\,(l)}, \qquad \Delta H_R < 0 \tag{1}$$

Three features dictate the structure of the model. First, the reaction is strongly exothermic, so the solid heats where reaction occurs, and since the rate is thermally activated the reaction is autocatalytic in temperature. Second, it proceeds through an aqueous film on the granule surface: with too little moisture the hydroxide is unavailable, with too much the pores flood, so the rate depends non-monotonically on solid moisture. This process is probably the reason why previous studies observed degradation of absorption capacity in pre-used and stored absorbents [5] . Third, it liberates water, which feeds back onto that same moisture dependence. The system is thus thermally and hygroscopically self-coupled, and it is this coupling, together with heat exchange at the canister wall, that produces the documented degradation of scrubber performance in cold conditions.

Stochastic initiation. At the scale of individual granules the reaction does not start everywhere at once. Whether a given domain of the bed begins to react depends on whether CO_2 reaches it and on whether its aqueous film is adequate, and a reacting domain may later be blocked by its own carbonate product, which strands unreacted hydroxide in its core. These events are random from granule to granule; their statistics, rather than a prescribed derating factor, determine how much of the nominal capacity is eventually used (Section 6). For years a five-minute prebreathe has been prescribed as a method for checking for abnormal behavior of the rebreather [6] . Here we can see that additionally, this procedure has a fundamental importance in the initiation of the reaction.

4. STATE SPACE AND SEMI-DISCRETIZATION

$x \in [0, L]$ is the arc length along the gas flow path, from the canister inlet ($x = 0$) to the outlet ($x = L$). The continuum state is the vector field

$$u(x,t) = \left(c,\ c_v,\ T_g,\ T_s,\ q,\ w\right)^T \tag{2}$$

with components: gas-phase CO_2 concentration c [mol m^{-3}]; gas-phase water vapor c_v [mol m^{-3}]; gas temperature T_g [K]; solid temperature T_s [K]; solid CO_2 loading q [mol kg^{-1}]; and solid moisture w [kg kg^{-1}]. The first three are advected by the gas flow; the solid temperature T_s is not advected but is spatially coupled through axial conduction; the last two, q and w, are local to the solid.

The path was partitioned into N cells of width Δx with centers x_i,

$$\Delta x = \frac{L}{N}, \qquad x_i = \left(i - \frac{1}{2}\right)\Delta x, \qquad i = 1, \ldots, N$$

where $y_i(t) \approx u(x_i, t)$ is the nodal value. Stacking the nodal values field by field gives the finite-dimensional state $y(t) \in \mathbb{R}^{6N}$; with $N = 30$ the model is a system of 180 coupled ODEs. This is the method of lines: space is discretized, time is left continuous, and the resulting object is a vector field on $\mathbb{R}^{6N}$. The construction is identical for every geometry, so that only the entries $A(x_i)$ and $\sigma(x_i)$ change. In Section 6 the solid fields q and w are carried by M discrete reactive domains in each cell, and y then denotes the gas fields together with the cell-averaged solid fields, conditional on one realization of the domain ensemble.

5. GOVERNING EQUATIONS

5.1 Interstitial gas velocity

Assuming a quasi-steady volumetric flow rate $\dot{Q}(t)$, uniform along the path, the interstitial (pore) gas velocity in a bed of void fraction ε and local cross-section $A(x)$ is

$$v(x,t) = \frac{\dot{Q}(t)}{\varepsilon\, A(x)}, \qquad \dot{Q} = \frac{\mathrm{d}V_{\mathrm{g}}}{\mathrm{d}t} \tag{3}$$

where V_{g} is the cumulative volume of gas passed through the canister, so that $\dot{Q}$ [m³ s⁻¹] is the volume passing per second. $\dot{Q}$ is built from ventilation and depth in Eq. (12b) and falls at depth, since the same number of moles occupies less volume. The quotient $v_{\mathrm{sup}} = \dot{Q}/A(x)$ is the *superficial* velocity — the speed the gas would have if the tube were empty. Because granules block most of the cross-section, the gas must pass through the open area $\varepsilon A(x)$ and speeds up accordingly; dividing by ε gives the *interstitial* velocity v, the true speed of the gas in the pore space, which actually carries CO_2, water vapor and heat downstream. The two differ by the factor $1/\varepsilon \approx 2.4$ for $\varepsilon = 0.42$.

The velocity is a derived quantity, not a parameter: it is computed at every node from $\dot{Q}$, ε and $A(x)$. It varies along x only if $A(x)$ does; beds of constant cross-section, such as both canisters treated here, have uniform v. It is the coefficient of the advection terms $-v\,\partial/\partial x$ in Eqs. (4a)–(4c) and sets how fast the reaction and thermal fronts are pushed toward the outlet. The mean gas residence time in the bed is

$$t_{\mathrm{res}} = \int_0^L \frac{\mathrm{d}x}{v} = \frac{\varepsilon\, V_{\mathrm{bed}}}{\dot{Q}}$$

which reduces to L/v for a constant cross-section. Equation (3) rests on three assumptions: a steady, uniform mean flow (real breathing is oscillatory; see Section 13); plug flow, uniform across each cross-section; and uniform packing ε.

5.2 Balance equations

$\mathcal{R}(c, T_s, q, w)$ denotes the specific reaction rate [mol CO_2 kg^{-1} s^{-1}], and the phase-conversion factor is introduced as

$$G = \frac{(1-\varepsilon)}{\varepsilon}\,\rho_s$$

[kg of solid per m^3 of gas void], which converts a rate per kilogram of solid into a source per cubic meter of void. The balances are

$$\frac{\partial c}{\partial t} = -v\,\frac{\partial c}{\partial x} + D\,\frac{\partial^2 c}{\partial x^2} - G\,\mathcal{R} \tag{4a}$$

$$\frac{\partial c_v}{\partial t} = -v\,\frac{\partial c_v}{\partial x} + D\,\frac{\partial^2 c_v}{\partial x^2} + \Gamma \tag{4b}$$

$$\frac{\partial T_g}{\partial t} = -v\,\frac{\partial T_g}{\partial x} + \alpha_g\,\frac{\partial^2 T_g}{\partial x^2} + h_v\,\frac{(T_s - T_g)}{\varepsilon\,\rho_m\,C_{p,g}} \tag{4c}$$

$$\frac{\partial T_s}{\partial t} = \alpha_s\,\frac{\partial^2 T_s}{\partial x^2} - h_v\,\frac{(T_s - T_g)}{(1-\varepsilon)\,\rho_s\,C_{p,s}} + \mathcal{R}\,\frac{(-\Delta H_R)}{C_{p,s}} - \frac{(1-r)\,h_w\,\sigma(x)\,(T_s - T_\infty)}{(1-\varepsilon)\,\rho_s\,C_{p,s}} \tag{4d}$$

$$\frac{\partial q}{\partial t} = \mathcal{R} \tag{4e}$$

$$\frac{\partial w}{\partial t} = \left(\frac{M_w}{1000}\right)\mathcal{R} - \gamma \tag{4f}$$

The reaction rate $\mathcal{R}$. $\mathcal{R} = \mathcal{R}(c, T_s, q, w)$ is the moles of CO_2 captured per kilogram of absorbent per second at a given point in the bed. It is the single source term that couples the six fields: it removes CO_2 from the gas in (4a) (scaled by G into gas-void units), releases reaction heat in (4d), advances the solid loading in (4e) and produces water in (4f). It is the product of a thermally activated rate constant, a saturation factor that shuts the reaction off as a node fills, a moisture factor, and a first-order dependence on the local gas-phase CO_2 concentration:

$$\mathcal{R}(c, T_s, q, w) = k(T_s) \cdot f_{sat}(q) \cdot f_{moist}(w) \cdot c \ \geq 0 \tag{4g}$$

with $k(T_s)$ an Arrhenius rate constant, $f_{sat}(q)$ driving $\mathcal{R}$ to zero as the loading q reaches the usable capacity $\eta\, q_{max}$ (with η the utilization, an output; Section 6), and $f_{moist}(w)$ a Gaussian in solid moisture. The full closure is given in Section 6; here it suffices that $\mathcal{R} \geq 0$ always (a node can absorb but never release CO_2), which is what makes the loading q monotone in (4e). The fields q, w and the rate $\mathcal{R}$ of (4a)–(4g) are cell averages over the M reactive domains of each cell (Section 6).

In Eqs. (4a)–(4g), D is an effective axial dispersion coefficient, α_g and α_s are effective thermal diffusivities, h_v is a volumetric interphase heat-transfer coefficient, h_w a wall heat-transfer coefficient, ρ_m the gas molar density, $C_{p,g}$ (molar) and $C_{p,s}$ (mass-specific) the heat capacities, M_w the molar mass of water, and $T_\infty(t)$ the ambient water temperature. The geometric functionals $A(x)$ and $\sigma(x)$ are defined in Section 7; the jacket recovery factor $r \in [0,1]$ is the subject of Sections 4.4–4.5, with $r = 0$ recovering a bare wall exactly.

5.3 Moisture exchange and the water balance

The terms Γ and γ encode a conservation law that is easy to violate. Reaction (1) produces one mole of water per mole of CO_2 captured, and that water appears in the condensed phase, on the granule. It reaches the gas only by evaporation. Accordingly, the reaction source appears once, in (4f), and never in (4b). The exchange between phases is a single physical flux written in two-unit systems:

$$\gamma = k_e(w - w^*) \qquad [\text{kg kg}^{-1}\ \text{s}^{-1}] \tag{5a}$$

$$\Gamma = \gamma \left(\frac{1000}{M_w}\right) G \qquad \left[\text{mol m}_{\text{void}}^{-3}\ \text{s}^{-1}\right] \tag{5b}$$

with w^* the moisture set-point and k_e an exchange rate. Because Γ is the image of γ under the unit conversion, and not an independent closure, the water leaving the solid is exactly the water entering the gas. The set-point of each reactive domain is its hygroscopic equilibrium moisture rather than a single value (Table A3).

The role of M_w. The reaction rate $\mathcal{R}$ is expressed in moles of CO_2 per kilogram of solid per second, and reaction (1) yields one mole of water per mole of CO_2 captured, so water is produced at $\mathcal{R}$ mol kg^{-1} s^{-1}. The solid moisture w, however, is a mass fraction (kg water per kg solid). To add a molar production rate to a mass-based quantity, moles of water must be converted to kilograms:

$$\mathcal{R}\ [\mathrm{mol_{H_2O}\ kg^{-1}\ s^{-1}}] \times M_{\mathrm{w}}\ [\mathrm{g\ mol^{-1}}] \div 1000\ [\mathrm{g\ kg^{-1}}] = [\mathrm{kg_{H_2O}\ kg^{-1}\ s^{-1}}]$$

so $(M_{\mathrm{w}}/1000)\,\mathcal{R}$ in (4f) is the rate at which reaction water accumulates on the solid, in the units of $\partial w/\partial t$; the second term, $-\gamma$, removes that water by evaporation into the gas. In (5b) the factor appears inverted, $1000/M_{\mathrm{w}}$, converting the mass-based evaporation flux back into a molar source for the gas-phase vapor. The reciprocal pairing is deliberate: it guarantees that the water leaving the solid equals the water entering the gas. Were M_{w} used inconsistently between the two equations, the model would create or destroy water. M_{w} is therefore a fixed physical constant, not a fitted parameter, whose only role is to bridge mole-based chemistry and mass-based moisture bookkeeping.

5.4 The wall boundary and the jacket recovery factor

The final term of (4d) is where the canister's thermal architecture enters. A bare wall would lose heat directly to water at T_∞ with strength $h_{\mathrm{w}}\,\sigma(x)$. A jacketed canister interposes a stream of warm returning gas between the wall and the water, so the wall exchanges with a warmer medium and through a larger resistance. This is represented by a single recovery factor $r \in [0,1]$ attenuating the wall loss:

$$\text{wall term} = -\frac{(1-r)\,h_{\mathrm{w}}\,\sigma(x)\,(T_{\mathrm{s}} - T_\infty)}{(1-\varepsilon)\,\rho_{\mathrm{s}}\,C_{p,s}} \tag{6a}$$

$r = 0$ is a bare wall against water and reduces (6a) exactly to the classical term; $r \to 1$ is a perfectly insulating jacket returning to the wall as much heat as it removes. Intermediate r models the real canisters. The factor is deliberately lumped: r is not resolved from a countercurrent heat-exchanger calculation but is a single number standing for the whole jacket. An equivalent, more explicit form replaces the sink temperature rather than the coefficient, writing the external medium at $T_{\mathrm{ext}} = T_\infty + r(\langle T_{\mathrm{s}}\rangle - T_\infty)$; to first order the two agree when the returning gas tracks the bed temperature, and the attenuation form is preferred because it needs no additional state.

5.5 An energy-balance bound

It is tempting to set r near unity on the grounds that the jacket is a good insulator. A steady-state energy balance shows that this is wrong, and by a wide margin.

At the EN 14143 injection rate, 1.6 L min⁻¹ STPD corresponds to $\dot{n}_{\mathrm{CO_2}} = 1.19 \times 10^{-3}$ mol s⁻¹ of CO_2, and with $\Delta H_{\mathrm{R}} \approx -70$ kJ mol⁻¹ the bed liberates about 83 W (net of the latent heat of the product water). That heat must leave. In this steady-state balance there are only two exits: the

wall and the gas. The gas is a poor exit — it enters at body temperature, already close to the bed temperature, so at 40 L min^{-1} it removes only of the order of 10 W of sensible heat. The wall must take essentially the rest. Writing the reaction heat load, the wall conductance and the steady bed temperature rise above the water,

$$\Phi_{\mathrm{rxn}} = \dot{n}_{\mathrm{CO_2}}\,(-\Delta H_{\mathrm{R}}), \qquad UA = (1-r)\,h_{\mathrm{w}}\,\sigma\,V_{\mathrm{bed}}, \qquad \Delta T = \frac{\Phi_{\mathrm{rxn}}}{UA} \tag{6b}$$

with $h_{\mathrm{w}} \approx 25$ W m^{-2} K^{-1} the bare-wall conductance is about 2.0 W K^{-1} for Shape 1 and 1.7 W K^{-1} for Shape 2.

6. THE SYSTEM AS A NON-AUTONOMOUS FLOW

When ∂_x is replaced by a first-order upwind difference (appropriate to the strongly advective regime) and ∂_x^2 by the standard three-point stencil, and a Dirichlet condition is imposed at the inlet and a zero-gradient condition at the outlet for the advected fields $(c, c_{\mathrm{v}}, T_{\mathrm{g}})$, Eqs. (4) become a coupled system of ODEs. In compact form,

$$\dot{y} = F(y, t; \theta, \Omega), \qquad y(0) = y_0, \qquad y \in \mathbb{R}^{6N} \tag{7}$$

where θ collects the physico-chemical parameters (including r) and Ω the geometric data (A, σ). Three structural remarks follow.

(i) The system is non-autonomous. Explicit time dependence enters only through the boundary data — the dive profile. Depth $d(t)$, water temperature $T_{\infty}(t)$, ventilation $\dot{V}_{\mathrm{E}}(t)$ and metabolic output $\dot{V}_{\mathrm{CO_2}}(t)$ are prescribed exogenous functions, $F(y,t) = \tilde{F}\big(y, \beta(t)\big)$ with $\beta(t) = \big(d, T_{\infty}, \dot{V}_{\mathrm{E}}, \dot{V}_{\mathrm{CO_2}}\big)(t)$. For a constant profile the system is autonomous and the reaction front is a travelling wave; for a real dive the front speed is modulated in time.

(ii) The dynamics are dissipative but not gradient-like. Heat is lost at the wall and CO_2 is convected out of the domain, so trajectories are bounded; yet the reaction supplies energy locally and the moisture closure introduces a non-monotone gain, so no Lyapunov function is proposed. The jacket weakens the dissipation at the wall but does not remove it unless $r = 1$ — and Sections 4.5 and 12.4 show that the boundedness of T_{s} in practice depends on r being small.

(iii) Part of the state is monotone. Since $\mathcal{R} \geq 0$ by construction, (4e) gives $\dot{q}_i \geq 0$ at every node: the loading coordinates are non-decreasing along any trajectory. The system has no non-trivial recurrence — no periodic orbits — and every trajectory is transient, approaching the exhausted state as $q \to \eta\, q_{\max}$, where η is the utilization that emerges from the stochastic events of Section 6. The scrubber is a one-shot device, and this holds for both geometries and every r, because neither A, σ nor r enters (4e).

(iv) The reaction layer is a random jump process superposed on the flow. Between events the vector field (7) is deterministic; at an event a reactive domain changes state (dormant to active, or active to passivated), which changes the source terms of (4a)–(4f) discontinuously. The system (7) is therefore conditional on a realization of the domain ensemble, each Monte Carlo run produces one trajectory, and the breakthrough time τ of Section 9 is a random variable whose distribution is obtained from the ensemble of trajectories.

7. REACTION RATE

The specific rate (4g) is restated here with its factors:

$$\mathcal{R}(c, T_s, q, w) = k(T_s) \cdot f_{sat}(q) \cdot f_{moist}(w) \cdot c \tag{8}$$

$$k(T_s) = k_0 \cdot \exp\left[-\frac{E_a}{R}\left(\frac{1}{T_s} - \frac{1}{T_{ref}}\right)\right] \tag{9a}$$

$$f_{sat}(q) = \left[\max\left(0{,}1 - \frac{q}{q_{max}}\right)\right]^n \tag{9b}$$

$$f_{moist}(w) = \exp\left[-\frac{(w - w^*)^2}{2\,\sigma_w^2}\right] \tag{9c}$$

Here R is the universal gas constant. f_{sat} expresses depletion of reactive hydroxide within a reactive domain, whose loading is bounded by the true capacity q_{max}; no derating coefficient is imposed, and the utilization η emerges as an output, Eq. (9i). Eqs. (9a)–(9c) are evaluated for each reactive domain, with q its loading. The exponent n shapes how the rate decays as the local loading approaches the usable capacity: $n = 1$ gives linear depletion; $n > 1$ produces an earlier, more gradual decline; $n < 1$ keeps the rate high until the node is nearly exhausted and then shuts it off abruptly. The value of n is 2/3, which corresponds to a shrinking spherical core, and is adopted for the reactive domains. The Gaussian f_{moist} encodes the moisture optimum at w^* with width σ_w. The product form is a strong assumption — it presumes the three effects act independently — and is the closure most in need of empirical support.

Reactive domains and random initiation. The absorbent of each cell i is divided into M reactive domains $j = 1, \ldots, M$, each representing a group of granules, with mass $m_{i,j}$ ($\sum_j m_{i,j} = m_i$, the absorbent mass of the cell), grain size $d_{p,i,j}$, loading $q_{i,j}$ and moisture $w_{i,j}$. Each domain is in one of four states $s_{i,j}$: dormant (0), active (1), passivated (2) or exhausted (3), and only active domains react. A dormant domain becomes active when CO_2 reaches it and its aqueous film is suitable; this initiation is a random event with hazard

$$\lambda_{\text{init}}(i,j) = k_{\text{init}}\, k(T_{s,i}) f_{\text{moist}}(w_{i,j}) c_i \tag{9d}$$

where k_{init} is an initiation coefficient, so that the probability that a dormant domain is initiated during a time step Δt is $1 - \exp(-\lambda_{init}\,\Delta t)$. At the start of a run a domain is active with probability $f_{moist}(w_{i,j})$ and dormant otherwise. The rate of an active domain and the resulting cell-averaged rate are

$$\mathcal{R}_{i,j} = \delta_{s_{i,j},1}\, k(T_{s,i}) f_{\text{sat}}(q_{i,j}) f_{\text{moist}}(w_{i,j}) \frac{d_{p,0}}{d_{p,i,j}}\, c_i \tag{9e}$$

$$\mathcal{R}_i = \frac{1}{m_i} \sum_{j=1}^{M} m_{i,j}\ \mathcal{R}_{i,j} \tag{9f}$$

where $\delta_{s_{i,j},1}$ is the Kronecker delta, which restricts the rate to active domains, f_{sat} is the factor (9b) applied to the domain loading, and $d_{p,0}$ is a reference grain size (smaller domains react faster per unit mass). The cell-averaged rate $\mathcal{R}_i$ takes the place of $\mathcal{R}$ in (4a)–(4f).

Passivation. An active domain may be passivated: a carbonate crust forms on its surface and blocks the unreacted hydroxide in its core, so that the domain stops reacting at a conversion $X = q_{i,j}/q_{\max} < 1$. The probability that an active domain is passivated while its conversion advances by dX is

$$\mathrm{d}\Pi_{\text{pass}} = h_0\, X^b \left(1 + a_w\, \zeta_{i,j}\right) \mathrm{d}X \tag{9g}$$

$$\zeta_{i,j} = -\ln f_{\text{moist}}(w_{i,j}) = \frac{\left(w_{i,j} - w^*\right)^2}{2\,\sigma_w^2} \tag{9h}$$

where h_0 and b are the coefficient and the conversion exponent of the passivation hazard and a_w weights the moisture stress $\zeta_{i,j}$, the departure of the domain moisture from its optimum. For a constant ζ the probability that a domain survives to a conversion X without passivation is $\exp\left[-h_0(1 + a_w\zeta)\frac{X^{b+1}}{b+1}\right]$, so that passivation strands a random part of the capacity of each domain. Domains that reach $X = 1$ are exhausted. At the breakthrough time τ (Section 9) the rated capacity is thus divided into four parts: capacity that has been used, capacity still held by active domains in the reaction front, capacity stranded in passivated domains, and capacity of domains never initiated. The utilization is the used part,

$$\eta = \frac{1}{q_{\max}\, m} \sum_{i=1}^{N} \sum_{j=1}^{M} m_{i,j}\ q_{i,j}(\tau) \tag{9i}$$

and is an output of the simulation: it is not imposed.

Heterogeneity and ensemble. Randomness enters through the initial condition of the domain ensemble. The domain masses follow from lognormally distributed grain sizes ($m_{i,j} \propto d_{p,i,j}^3$ within a cell). The initial moisture of a domain is the sum of a run-level offset (one draw per canister, representing differences of batch, storage and packing), a component correlated along the flow path (first-order autoregressive, with a correlation coefficient of 0.8 between neighboring cells) and an independent domain-level component; a lognormally distributed hygroscopicity factor $\chi_{i,j}$ (mean 1) scales the equilibrium moisture of each domain, so that moisture heterogeneity persists during the run. Each Monte Carlo run is one independent realization of the ensemble, i.e. one possible life of one canister, and the distribution of τ and η over runs measures the variability between nominally identical canisters. The parameter values are listed in Table A3.

Physical basis of the passivation coefficient. The coefficient h_0 lumps the processes by which unreacted hydroxide becomes inaccessible once part of a reactive domain has been converted. These include the growth of a carbonate layer that lengthens the diffusion path to the granule core, the plugging of fine pore throats by a product of larger molar volume than the reactant, and the dependence of both on the aqueous film in which the reaction proceeds. The film is thinned by drying and flooded by excess moisture, and the water formed by the reaction itself, together with condensation in a cold bed, tends to displace the moisture above its optimum as conversion advances; this dependence is represented by the moisture-stress term of (9g). Grain size, pore structure, the alkali-promoter content and its depletion, storage history and lot-to-lot variation are expected to shift h_0 but are not resolved. Temperature, local reaction rate and rest periods are also expected to influence passivation but do not enter h_0 in the present formulation, in which the hazard depends only on conversion and moisture. Because these factors cannot be separated with the available data, h_0 is treated as an uncalibrated lumped parameter that sets the stranded capacity, and the emergent utilization is conditional on its assumed value. Direct constraints would come from the residual hydroxide of spent granules along the flow path (titration or thermogravimetry), from granule cross-sections showing unreacted cores and crust thickness, and from breakthrough measurements at two or more temperatures and flows, which separate h_0 from k_0.

Absorbent grade enters through capacity and relative grain size. Both canisters are charged with Sofnolime 797 [7] , rated at roughly 150 L CO_2 kg^{-1}, i.e. $q_{\max} \approx 6.7$ mol kg^{-1}. Grain size in principle affects intraparticle-diffusion limitation and hence front sharpness, but the model lumps the granule (Section 13): $\mathcal{R}$ is a granule-averaged rate with no intraparticle-diffusion length, so grain size cannot enter through intraparticle diffusion here. Grain size enters only relatively,

through the factor $d_{p,0}/d_{p,i,j}$ of (9e), which makes smaller domains react faster per unit mass; the absolute reference size $d_{p,0}$ cancels and is carried for documentation only. Because the grade is common to both units, any difference the model predicts between them arises from geometry, charge and jacket alone.

The thermal coupling is a feedback loop. Reaction raises T_s through $\mathcal{R}(-\Delta H_R)/C_{p,s}$; higher T_s raises $k(T_s)$; higher k raises $\mathcal{R}$. This positive loop is arrested by f_{sat}, which drives $\mathcal{R}$ to zero as the node exhausts, and opposed by the wall loss (6a). Cold water strengthens the opposing term, depressing T_s and hence k, which broadens the reaction zone and shortens the useful life of the bed — the cold-water penalty. The jacket weakens that opposing term, so a jacketed canister suffers a smaller cold-water penalty than a bare one of the same (A, σ). In the model this is a deformation of the vector field through a single scalar rather than an added correction; but by Sections 4.5 and 12.4 the admissible deformation is modest, and with it the predicted benefit is correspondingly modest — of the order of a few percent in breakthrough time, not a transformation.

8. GEOMETRY AS A PARAMETER OF THE VECTOR FIELD

The canister enters (4) through exactly two functionals of the flow coordinate: the cross-sectional area $A(x)$, which sets the advective velocity via (3), and the specific wall area $\sigma(x)$ = (wall area exchanging heat)/(bed volume) [m⁻¹], which sets the strength of the wall coupling. For any prismatic bed — a constant cross-section swept along the flow direction — the side-wall area is the section perimeter $\mathcal{P}$ times the flow length and the bed volume is the section area A times the flow length, so $\sigma = \mathcal{P}/A$ independently of the flow length. This single expression contains the circular and stadium cases and reduces to the familiar $4/d$ for a circle (Table 1).

Table 1. Geometric functionals for the two canister formats. ℓ and W are the overall length and width of the stadium section ($\ell \geq W$).

Format	$A(x)$	$\sigma(x)$	Reaction front
Axial, circular (Shape 1)	$\pi d^2/4$ (constant)	$4/d$ $(= \mathcal{P}/A)$	plane along axis
Axial, stadium (Shape 2)	$(\ell - W)W + \pi(W/2)^2$ (constant)	$\mathcal{P}/A$, $\mathcal{P} = 2(\ell - W) + \pi W$	plane along axis

8.1 Mass consistency

The bed volume is the integral of the cross-section along the path, $V_{bed} = \int_0^L A(x)\,dx \approx \sum_i A(x_i)\,\Delta x$. The absorbent charge m is a measured quantity, and the solid-phase density is therefore not free:

$$\rho_s = \frac{m}{(1-\varepsilon)\,V_{bed}} \tag{10}$$

Total capacity scales as $\eta\, q_{max}\, m$ (with η the emergent utilization), so the charge must be imposed rather than inferred: ρ_s is derived from (10) at load time, with m and ε as free inputs. Comparing two geometries at fixed m rather than fixed ρ_s is essential, or one compares canister sizes rather than canister designs. Sized from their measured internal dimensions and charges, the two units land at almost identical bulk density (Table 2) — a useful cross-check, since a plain rectangular box of Shape 2 envelope would imply a bulk density too low for packed Sofnolime.

Table 2. Bed dimensions, charge and derived quantities. Both at $\varepsilon = 0.42$, both Sofnolime 797, both jacketed.

Canister	Bed section	V_{bed} (L)	m (kg)	Bulk density (kg m^{-3})	σ (m^{-1})	Wall area (m^2)
Shape 1	circle, d = 15 cm × L = 17 cm	3.00	2.50	832	26.67	0.0801
Shape 2	stadium 28 × 11 cm, flow 10 cm	2.82	2.35	833	24.31	0.0686

9. BOUNDARY FORCING, REFERENCE CONDITIONS AND DEPTH

The inlet condition supplies the Dirichlet data $(c, c_v, T_g)|_{x=0}$. The ambient pressure in atmospheres absolute is denoted $P(t)$. Metabolic production and ventilation are prescribed as molar rates, independent of depth: the diver's tissues produce a fixed number of moles of CO_2 per minute and the lungs move a fixed number of moles of gas per minute, irrespective of ambient pressure. CO_2 injection specified by EN 14143 is conventionally an STPD volume, to be converted with the STPD molar volume $V_m(T_0) = 22.414$ L mol^{-1}. Ventilation is a body/loop flow, converted with the body-temperature molar volume $V_m(T_b) \approx 25.45$ L mol^{-1}, where $V_m(T) = RT/P_{atm}$ at 1 atm. Converting the CO_2 at body temperature instead understates the molar CO_2 load by about 12 % and, because breakthrough is capacity-limited (Section 9.1), delays the predicted breakthrough by about 13–14 %. Hence

$$\dot{n}_{tot} = \frac{\dot{V}_E}{V_m(T_b)}, \qquad \dot{n}_{CO_2} = \frac{\dot{V}_{CO_2}}{V_m(T_0)} \tag{11}$$

$$P(t) = 1 + \frac{d(t)}{10} \tag{12a}$$

$$\dot{Q}(t) = \frac{\dot{n}_{tot}\, R\, T_b}{P(t)\, P_{atm}}, \qquad c(0,t) = \frac{\dot{n}_{CO_2}}{\dot{Q}(t)} \tag{12b}$$

$$\rho_{\mathrm{m}} = \frac{P(t)\,P_{\mathrm{atm}}}{R\,T_{\mathrm{g}}} \tag{12c}$$

The molar CO_2 load per unit time, $\dot{Q}\,c(0,t) = \dot{n}_{\mathrm{CO_2}}$, is invariant. Depth does not change how much CO_2 must be absorbed; it changes the gas density in which that CO_2 is delivered and hence, through (8), the local rate and the sharpness of the front. Equation (12c) likewise makes the gas molar density, and with it the gas heat capacity per unit volume in (4c), rise with depth. Pressures are carried in atmospheres absolute throughout and converted to pascals, through P_{atm}, only inside the ideal-gas law.

10. BREAKTHROUGH AS A FIRST-HITTING TIME

Breakthrough is not a property of the state vector but of a scalar observable of it. The exit partial pressure of CO_2 at the outlet node N is defined as:

$$h(y) = \frac{c_N\,R\,T_{\mathrm{g},N}}{P_{\mathrm{atm}}} \qquad [\mathrm{ATA}] \tag{13}$$

Breakthrough is defined by the threshold $p^* = 0.005$ ATA (≈ 0.5 kPa); the breakthrough time is the first-hitting time of the super-level set of h:

$$\tau(p^*) = \inf\{t > 0:\ h(\varphi_t(y_0)) \geq p^*\} \tag{14}$$

where φ_t is the (non-autonomous) flow map of (7). Three things are explicit. The threshold p^* is a modeling choice, not a physical constant, so τ is a function of it, and sensitivities should be reported as $\tau(p^*)$ over a range. The event is a codimension-one surface $\{h = p^*\}$ in $\mathbb{R}^{6N}$, and τ is finite because, by the monotonicity of q (Section 5(iii)), the bed necessarily exhausts. And τ depends on the full forcing history $\beta(\cdot)$ on $[0,\tau]$, not on its instantaneous value: a cold, hard-working period early in a dive is not equivalent to the same period late in it. The definition is identical for both canisters; geometry and jacket change where the surface lies, not what it is. τ is a random variable: each realization of the domain ensemble yields one value, and the distribution of τ over realizations is what is reported (Section 12).

10.1 Breakthrough is capacity-limited

Because the front is comparatively sharp, the exit partial pressure stays low until the bed is nearly full and then rises over some minutes (Section 12.2). To a good approximation the breakthrough time is therefore set by a simple ratio,

$$\tau \approx \frac{\eta\,q_{\max}\,m}{\dot{n}_{\mathrm{CO_2}}} \tag{15}$$

which makes τ inversely proportional to the metabolic load and only weakly dependent on everything else. This is the single most important fact for interpreting a reported duration, and the easiest way to be misled. Section 12.2 (Table 4) quantifies this dependence for the two canisters. A duration quoted without its CO_2 rate is close to meaningless, and a long duration obtained at a light load is not evidence that a model is broken.

11. NUMERICAL TREATMENT

The semi-discrete system (7) is stiff: reaction and interphase heat-transfer time scales are orders of magnitude shorter than the hours-long saturation of the bed, and the diffusive stencils contribute eigenvalues scaling as Δx^{-2}. Explicit integrators are impractical for the fully coupled system. The gas fields are therefore treated as quasi-steady, as described below.

Advective terms use first-order upwinding, which is unconditionally monotone — it does not produce spurious oscillations or negative concentrations ahead of the front — but introduces numerical diffusion that broadens the reaction zone. Since front sharpness underwrites the capacity-limited approximation (15), the resolution N should be varied to confirm that conclusions are not artifacts of that diffusion (Section 12.3). Diffusive terms use a three-point stencil with a ghost node carrying the inlet value at $x = 0$ and a zero-gradient ghost at $x = L$; the solid temperature, which is not advected, receives zero-gradient conditions at both ends. The rate (8) and f_{sat} are clipped at zero so that an exhausted node cannot regenerate. The total absorbed CO_2 is checked against $\int \dot{n}_{CO_2}\, dt$ and the water balance against (5).

The gas residence time in the bed, t_{res} (Section 4.1), is of the order of seconds to tens of seconds (Section 12.1), more than two orders of magnitude shorter than the time over which the solid state changes (the reaction front crosses the bed in hours). The gas fields were therefore treated as quasi-steady at each time step and obtained by upwind-implicit marching through the cells; for the CO_2 field this gives

$$\frac{c_i}{\rho_{m,i}} = \frac{c_{i-1}/\rho_{m,i-1}}{1 + S_i/\dot{Q}_i} \tag{16}$$

$$S_i = k(T_{s,i}) \sum_{j=1}^{M} m_{i,j}\ \delta_{s_{i,j},1}\, f_{\mathrm{sat}}(q_{i,j}) f_{\mathrm{moist}}(w_{i,j}) \frac{d_{p,0}}{d_{p,i,j}} \tag{17}$$

where S_i [m³ s⁻¹] is the volumetric flow of gas cleaned per second by the active domains of cell i and $\dot{Q}_i = \frac{\dot{n}_{tot}\, R\, T_{g,i}}{P\, P_{atm}}$ is the local volumetric flow. The gas temperature and the vapor fields were marched in the same way. With the inspired CO_2 recirculated into the next exhalation, the inlet

mole fraction follows from the product of the cell factors of (16). The solid state was advanced with a fixed step $\Delta t = 5$ s: the CO_2 taken up by each domain, its moisture and its temperature were updated explicitly, the conduction and wall-loss terms of (4d) implicitly, and the random events of initiation and passivation were sampled once per step from the probabilities $1 - \exp(-\lambda_{init}\Delta t)$ and $1 - \exp[-h_0 X^b (1 + a_w \zeta)\Delta X]$, where ΔX is the conversion increment of the step.

Monte Carlo ensemble and statistics. Each canister was simulated 40 times with independent random seeds (distinct seed ranges for the two canisters), and every run drew the domain ensemble afresh. The outcomes of each run (τ, η) were summarized by their mean, standard deviation, coefficient of variation and 5th, 50th and 95th percentiles, and the two canisters were compared with Welch's t-test and with the probability that a randomly chosen run of one canister exceeds a randomly chosen run of the other. The number of domains per cell, $M = 50$, is part of the variability model, since each domain is an independent unit (Section 12.3).

12. PARAMETERS AND CALIBRATION STATUS

A model whose structure is sound but whose kinetics are guessed can be trusted for the direction and rough magnitude of a sensitivity, not for an absolute duration. The parameter values are given in Appendix A.

A defensible calibration would fit the kinetic and transport parameters (k_0, E_a and the diffusivities) to bench breakthrough curves at two or more water temperatures and at least two work rates, holding the measured quantities fixed, and validate against a held-out condition. The utilization η is not a parameter: it emerges from the stochastic parameters (k_{init}, h_0, b, a_w and the heterogeneity parameters of Table A3), which should be constrained by the measured utilization and by its scatter between nominally identical canisters. The pair $(1 - r)$ and h_w should be fitted together, ideally against a measured bed temperature, since only their product is identifiable from breakthrough data alone. Until the kinetics are fitted, the model expresses the structure of the problem, not its numbers.

13. RESULTS

13.1 Simulated conditions and ensemble

The stochastic model was run for the two canisters of Table 2 under the EN 14143 baseline: a constant depth of 100 m ($P = 11$ ATA), water at 4 °C, a metabolic CO_2 production of 1.6 L min^{-1} (STPD) and a breathing frequency of 20 min^{-1} with a tidal volume of 2.0 L, i.e. a

ventilation of 40 L min^{-1}. The ensemble comprised 40 independent Monte Carlo runs per canister (seeds 1–40 for Shape 1 and 100001–100040 for Shape 2), with $N = 30$ cells, $M = 50$ reactive domains per cell, a time step of 5 s, $r = 0.25$ and $h_w = 200$ W m^{-2} K^{-1}, and the other parameter values of Appendix A (Tables A1, A2 and A3). A run was stopped when the inspired CO_2 partial pressure reached 0.015 ATA (≈ 1.5 kPa), and breakthrough was recorded at the first crossing of $p^* = 0.005$ ATA (≈ 0.5 kPa), Eq. (14). All 80 runs reached breakthrough.

At this depth the volumetric flow through the bed was 6.06×10^{-5} m^3 s^{-1} (3.6 L min^{-1}), corresponding by Eq. (3) to interstitial velocities of 0.82 cm s^{-1} (Shape 1) and 0.51 cm s^{-1} (Shape 2) and to gas residence times of 20.8 s and 19.5 s. The molar CO_2 delivery rate was $\dot{n}_{CO_2} = 1.190 \times 10^{-3}$ mol s^{-1} (Eq. 11, STPD molar volume).

13.2 Breakthrough time and emergent utilization

The inspired CO_2 partial pressure rose gradually before crossing the threshold (Fig. 1): the median exit pressure at 100 min was 0.007 kPa for Shape 1 and 0.014 kPa for Shape 2, and the rise from 0.1 kPa to the threshold took 18.0 ± 1.4 and 17.4 ± 1.1 min, respectively.

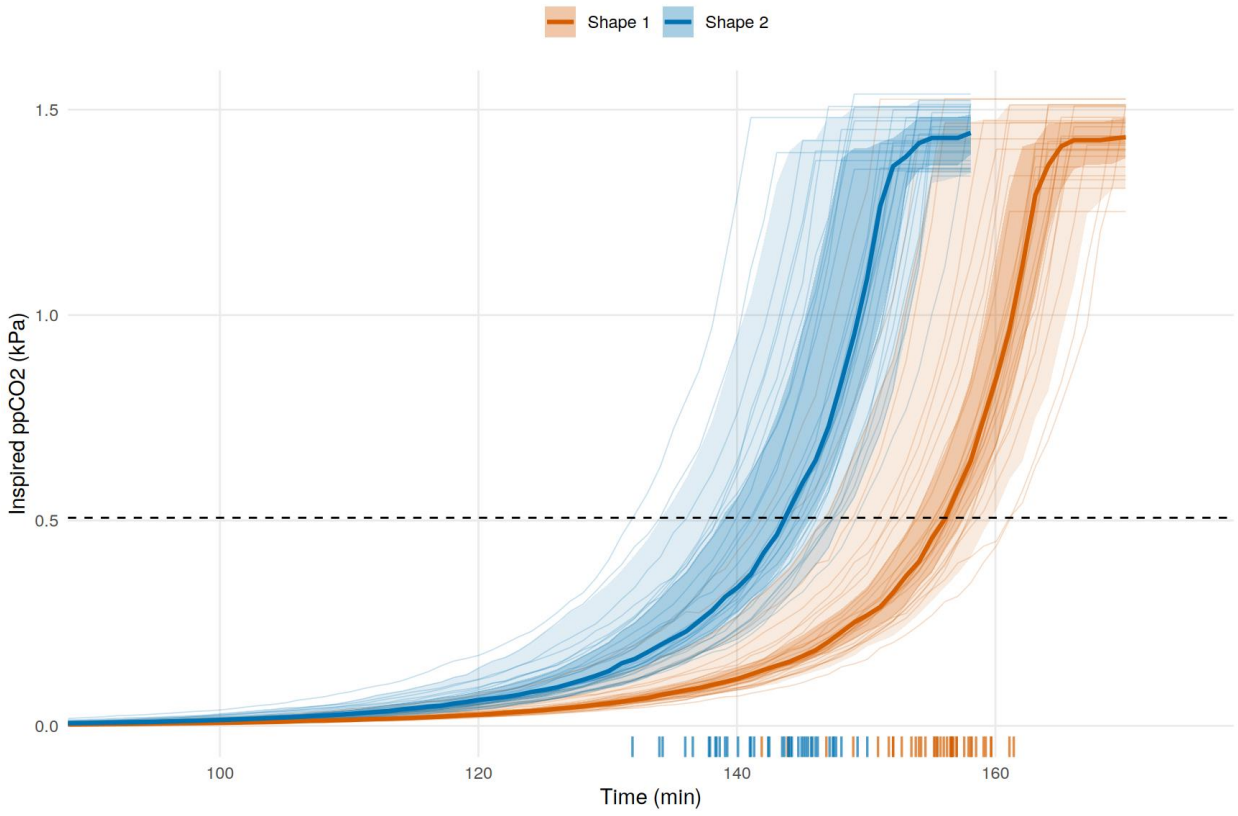

Figure 1. Inspired CO_2 partial pressure at the canister outlet for 40 Monte Carlo runs per canister. Thin lines: 30 individual runs; thick lines: median; dark and light bands: 25–75 % and 5–95 % ranges; ticks: breakthrough time of each run; dashed line: threshold p^* ≈ 0.5 kPa. Runs were stopped at 0.015 ATA (≈ 1.5 kPa) and their last value is carried forward.

Breakthrough occurred at $\tau = 155.1 \pm 4.2$ min for Shape 1 and 142.5 ± 4.5 min for Shape 2 (mean ± standard deviation over 40 runs; Table 3, Fig. 2), a coefficient of variation of about 3 %. The 5th percentile of τ, more relevant to planning than the mean, was 146.8 and 134.2 min. The utilization that emerged at breakthrough was $\eta = 0.662 \pm 0.018$ and 0.647 ± 0.020, i.e. about 66 % and 65 % of the rated capacity $q_{\max}\, m$.

Table 3. Breakthrough time τ and emergent utilization η at breakthrough over 40 Monte Carlo runs per canister (EN 14143 baseline: 100 m, 4 °C, 40 L min⁻¹, CO_2 1.6 L min⁻¹). Values are mean ± standard deviation, with the 5th, 50th and 95th percentiles in brackets.

Quantity	Shape 1 (axial)	Shape 2 (stadium)
τ (min)	155.1 ± 4.2 (146.8 / 156.1 / 159.7)	142.5 ± 4.5 (134.2 / 143.8 / 148.1)
Coefficient of variation of τ (%)	2.7	3.1
τ per kg of absorbent (min kg⁻¹)	62.1 ± 1.7	60.7 ± 1.9
η	0.662 ± 0.018 (0.626 / 0.666 / 0.682)	0.647 ± 0.020 (0.609 / 0.653 / 0.672)
Time from 0.1 kPa to p^* (min)	18.0 ± 1.4	17.4 ± 1.1

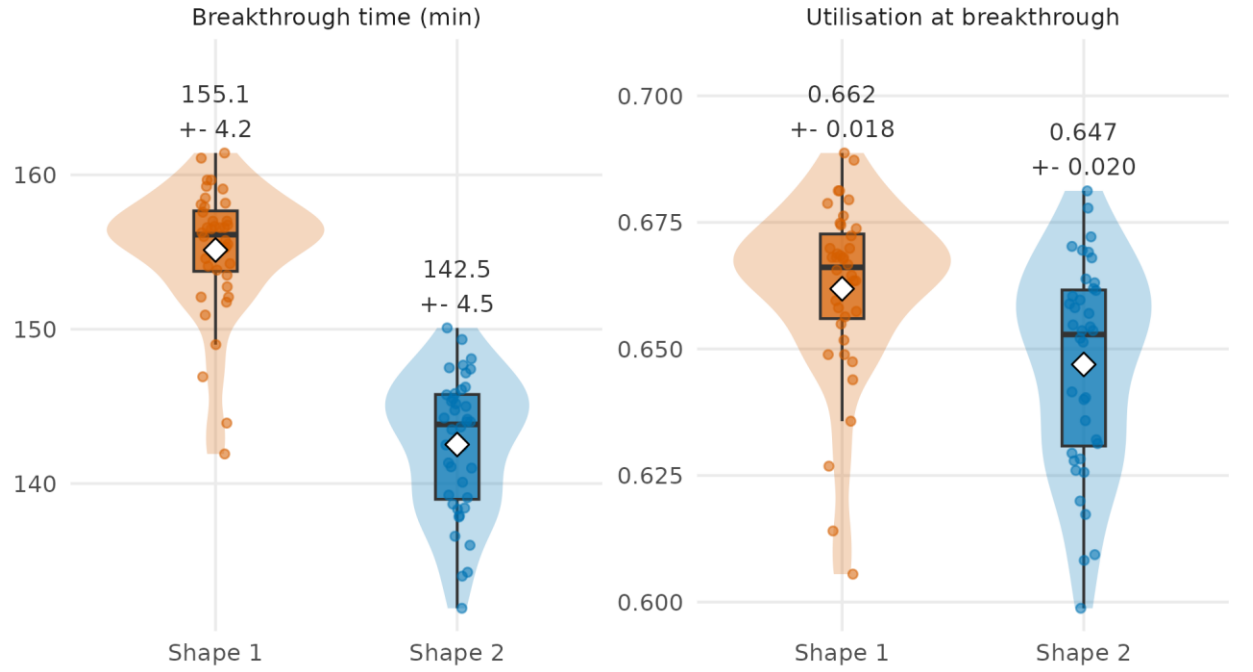

Figure 2. Distributions of breakthrough time (left) and utilization at breakthrough (right) over 40 runs per canister. Dots: individual runs; box: quartiles; diamond and label: mean ± standard deviation; shaded outline: kernel density.

Shape 1 reached a slightly higher utilization than Shape 2 (difference in mean η 0.015; 95 % CI 0.006 to 0.023; p-value = 0.0008), and its breakthrough time was 12.6 min longer (95 % CI 10.7–14.5 min; p-value = 3×10^{-21}); a random Shape 1 run outlasted a random Shape 2 run in 97 % of pairings. Most of the difference reflected the absorbent charge: the ratio of the mean durations (1.088) exceeded the ratio of the charges (2.50/2.35 = 1.064) by only 2.3 %.

The duration is set mainly by the metabolic load (Eq. 15, Table 4): Shape 2 broke through after about 143 min at 1.6 L min^{-1}, about 211 min at 1.0 L min^{-1} and about 274 min at a resting 0.75 L min^{-1}, a nearly twofold spread produced by the scenario alone. It's important to note that EN 14143 parameters would mean a level of physical effort during the dive that would be equivalent to exercising at, or slightly above, the anaerobic threshold for most of the population [8] , which is unrealistic and excessively conservative.

Table 4. Breakthrough time τ (min) and, in brackets, utilization η at three CO_2 loads (100 m, 4 °C, 40 L min^{-1}; mean of 40 runs at 1.6 L min^{-1} and of 12 runs at 1.0 and 0.75 L min^{-1}). The values at 1.6 L min^{-1} are those of Table 3; the others are additional runs of the same model, with uncalibrated parameters.

$\dot{V}_{CO_2}$ (L min^{-1} STPD)	Shape 1 τ (min)	Shape 2 τ (min)	Regime
1.6 (EN 14143)	155.1 (0.662)	142.5 (0.647)	standardized test
1.0	225.4 (0.601)	210.8 (0.598)	moderate work
0.75	291.2 (0.582)	273.8 (0.583)	light / resting

13.3 Consistency checks and numerical verification

The CO_2 balance closed to within 5.0×10^{-9} (relative) for Shape 1 and 4.5×10^{-15} for Shape 2, and the water balance to within 8.2×10^{-16} kg in all 80 runs. Eq. (15), evaluated with the emergent utilization and the STPD CO_2 delivery rate, reproduced τ in every run (largest relative deviation 5×10^{-9}): all the CO_2 delivered before breakthrough was absorbed.

The numerical scheme of Section 10 was verified in additional runs. The quasi-steady treatment of the gas was compared with a full co-simulation in which the gas transport was integrated dynamically with sub-steps of 0.05 s: for three paired realizations per canister the breakthrough times agreed to within 0.4 min (0.3 %). Halving or doubling the time step (2.5 and 10 s) changed the ensemble-mean breakthrough time by less than 0.5 % (24 paired runs per canister).

The spatial resolution was not converged at $N = 30$: for Shape 1 the mean breakthrough time was 155.1 min at $N = 30$, 162.0 ± 4.3 min at $N = 60$ (40 runs; η = 0.691) and 165.9 min at $N = 120$ (16 runs; η = 0.708), and for Shape 2 142.5, 147.9 ± 4.1 (η = 0.671) and 153.0 min (η = 0.694), as expected from the numerical diffusion of first-order upwinding. The $N = 30$ results

are therefore conservative, by about 4 % relative to $N = 60$ and 7 % relative to $N = 120$, whereas Shape 1 outlasted Shape 2 at every resolution (by 12.6, 14.2 and 12.9 min).

13.4 Sensitivity to the jacket factor

Figure 3 shows that only small r values, roughly 0.1 to 0.3, are possible: larger values give unrealistic bed temperatures (open symbols).

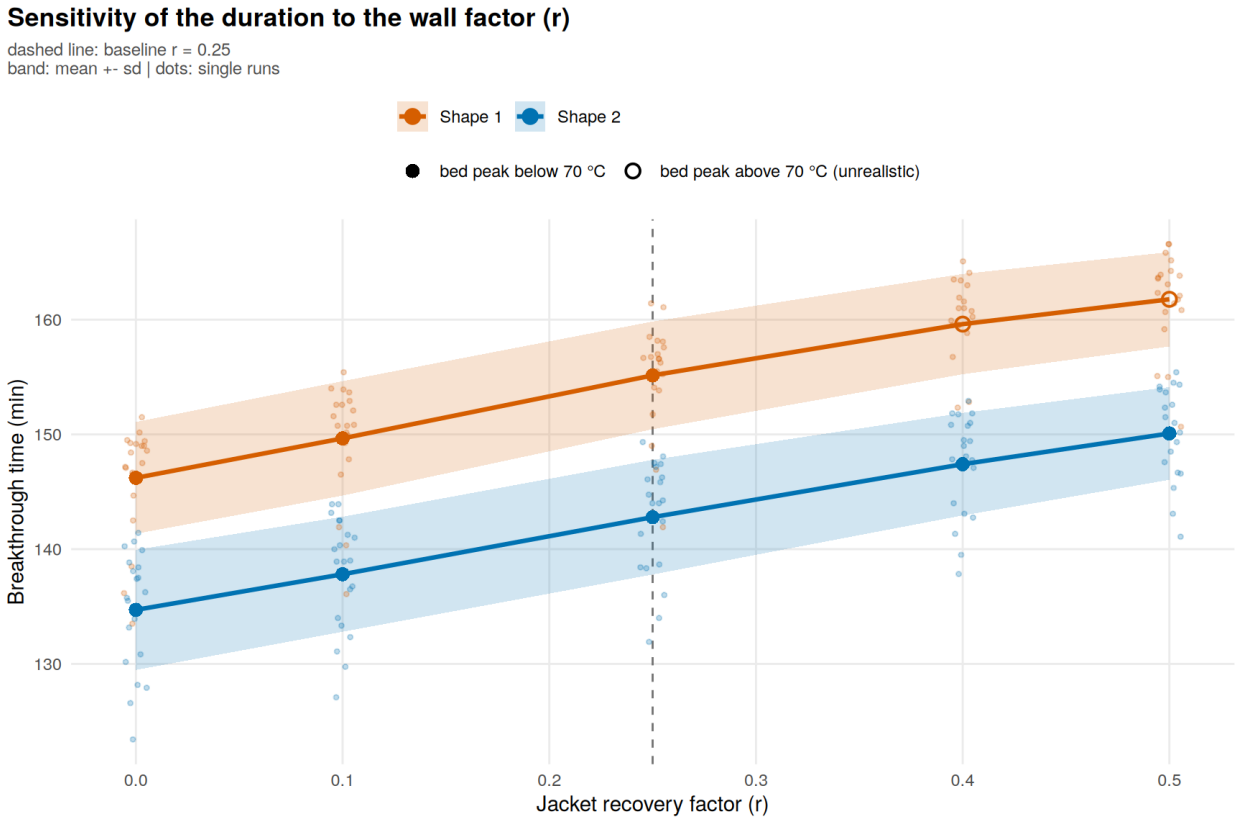

Figure 3. Sensitivity of the breakthrough time to the jacket recovery factor r (EN 14143 baseline; 20 runs per canister and value of r, same seeds). Dashed line: baseline r = 0.25; band: mean ± standard deviation; dots: single runs; open symbols: bed peak above 70 °C (unrealistic).

14. LIMITATIONS

Latent heat. Evaporation and condensation exchange latent heat with the solid, and with ≈ 44 kJ mol^{-1} of vaporization the latent term is large against the ≈ 83 W the reaction liberates. Its size is strongly depth-dependent, because it scales with the vapor mole fraction and hence inversely with ambient pressure. The closures involved — the hygroscopic equilibrium set-point (Table A3), instantaneous condensation at saturation and the drainage limit — are lumped and uncalibrated.

Lumped jacket. r is one scalar standing for a countercurrent heat exchanger whose recovery varies along the flow path and with flow rate. It is effective and uncalibrated, and only $(1-r)\,h_{\mathrm{w}}$ is identifiable from breakthrough data.

One-dimensionality. Channeling, wall bypass and gravitational settling are inherently multi-dimensional; they are not resolved, and the emergent utilization η contains no contribution from them, since all the domains of a cell see the same gas. In a large-frontal-area, short bed such as the stadium section, flow maldistribution across the wide face is exactly the effect that the emergent utilization η cannot resolve, and it is the most likely source of real differences between the two canisters beyond those shown in Section 12.

Steady flow. Breathing is oscillatory; the model advects with a mean flow $\dot{Q}$. Tidal reversal within the bed and the associated axial mixing are not represented.

Independent closures. The product form (8) assumes that thermal, saturation and moisture effects do not interact. Pore flooding beyond the moisture factor, and channel formation late in bed life, are outside the model.

Lumped granule. Intraparticle diffusion is not resolved, and the shrinking-core structure of individual granules is represented only through the factor $(1-X)^{2/3}$ of the domain rate and the relative grain size $d_{p,0}/d_{p,i,j}$, so absorbent grade enters through capacity and, only weakly, through front sharpness.

Uncalibrated kinetics. Absolute breakthrough times carry no warranty. The model predicts capacity and endurance from $q_{\max}$, m and the stochastic domain parameters, which determine the emergent η; a published certified endurance is only an external comparison and is itself a conservative maximum operating duration rather than a measured breakthrough. The model must not be used for dive planning or any life-support purpose.

Numerical resolution. The ensemble used $N = 30$ cells; the reported durations are conservative by about 4 % relative to $N = 60$ and 7 % relative to $N = 120$ (Section 12.3), and kinetic parameters calibrated at one resolution are not transferable to another.

Stochastic closure. The initiation and passivation laws (9d)–(9h) are phenomenological: their forms and the parameters k_{init}, h_0, b and a_w are uncalibrated, and the number of domains per cell M sets the run-to-run spread. Both the mean utilization and its variance therefore depend on closures that bench data must constrain; the emergent utilization of Section 12 is a property of the assumed parameters, not a measurement.

15. CONCLUSIONS

Casting the scrubber as a dynamical system clarifies what kind of object it is. The state is a point in $\mathbb{R}^{6N}$ (conditional on one realization of the stochastic domain ensemble); the canister geometry and absorbent chemistry define a vector field on that space; the dive profile forces it non-autonomously; the loading coordinates are monotone, so the flow is transient and terminates in an exhausted state; and breakthrough is the first-hitting time of a codimension-one surface defined by a scalar observable. Two real canisters — the axial-circular Shape 1 and the stadium-section Shape 2, both charged with Sofnolime 797 and both insulated by a return-gas jacket — are the same model at two settings of a small set of functionals: the cross-sectional area $A(x)$, the specific wall area $\sigma(x) = \mathcal{P}/A$ for a prismatic bed, and a scalar jacket-recovery factor r attenuating the wall loss.

Three results carry beyond the particular canisters. First, r is not a free dial: a steady-state energy balance against the ≈ 83 W the reaction liberates bounds it to roughly 0.1–0.3, and larger values produce bed temperatures that are physically impossible. Second, breakthrough is capacity-limited, so $\tau \approx \eta\, q_{\max}\, m/\dot{n}_{\mathrm{CO_2}}$ scales inversely with metabolic load; a duration quoted without its CO_2 rate is close to meaningless, and the nearly twofold spread between a resting and a working load is scenario, not model error. Third, capacity and endurance are outputs computed from a material specification, a measured mass and a stochastic description of reaction initiation and passivation (from which the utilization emerges), never numbers fed in — which is what allows a published endurance to serve as an independent check rather than a target. The formulation is sound and covers both geometries; the parameters are not yet calibrated, and that distinction should be preserved in any use of the model.

At the EN 14143 baseline (100 m, 4 °C, 20 breaths min^{-1} of 2.0 L, CO_2 1.6 L min^{-1}) Shape 1 and Shape 2 broke through at 155 ± 4 and 143 ± 4 min, with emergent utilizations of 0.66 and 0.65; the 8.8 % difference in duration slightly exceeded the 6.4 % difference in absorbent charge because Shape 1 was used somewhat more completely ($p = 0.0008$). The absolute values depend on the spatial resolution (conservative by about 4 % at $N = 30$ relative to $N = 60$) and on uncalibrated parameters, whereas the ranking of the canisters did not change.

REFERENCES

1. Clarke, J. R. Navy Experimental Diving Unit Physiological Event Prediction in Evaluations of Underwater Breathing Apparatus NAVY EXPERIMENTAL DIVING UNIT Distribution Statement A: Approved for Public Release, Distribution Unlimited. (2016).

2. Clarke, J. R. The Use of One-Sample Prediction Intervals for Estimating CO_2 Scrubber Canister Durations.
3. David Harvey, Neal W Pollock, Nicholas Gant, Jason Hart, Peter Mesley, Simon J Mitchell. The Duration of Two Carbon Dioxide Absorbents in a Closed-Circuit Rebreather Diving System. Diving Hyperb Med . 2016;46(2):92-7.
4. Gant, N., van Waart, H., Ashworth, E. T., Mesley, P. & Mitchell, S. J. Performance of cartridge and granular carbon dioxide absorbents in a closed-circuit diving rebreather. Diving Hyperb Med . 2019 Dec 20;49(4):298-303.
5. Pollock, N. W. et al. Storage of partly used closed-circuit rebreather carbon dioxide absorbent canisters. Diving Hyperb Med. 2018 Jun 27;48(2):96–101.
6. Deng, C. et al. The Five-Minute Prebreathe in Evaluating Carbon Dioxide Absorption in a Closed-Circuit Rebreather: A Randomized Single-Blind Study. Diving Hyperb Med. 2015;45(1):16-24.
7. Sofnolime-797-CD-TDS-v12 tech.
8. Asok Kumar Ghosh. Anaerobic Threshold - Its Concept and Role in Endurance Sport. Malays J Med Sci. 2004;11(1):24–36.

Appendix A. Parameter Values

Table A1. Absorbent and reaction-kinetics parameters.

Symbol	Meaning	Unit	How the value was defined (notes)
$q_{\max}$	Absorbent rated CO_2 capacity	mol CO_2 kg^{-1}	MATERIAL SPEC: Sofnolime 797 rated ~150 L kg^{-1} → 150/22.414 = 6.69. Same for both units.
η	Utilization (fraction of the rated capacity used at breakthrough)	dimensionless, (0, 1]	OUTPUT: emerges from the Monte Carlo events, Eq. (9i); 0.66 in the ensemble of Section 12. Neither set nor fitted.
k_0	Arrhenius pre-exponential factor	m^3 gas kg^{-1} s^{-1}	UNCALIBRATED [CALIBRATE]: 3.5×10^{-3} (at 1 ATA). Sets front sharpness.
E_a	Activation energy	J mol^{-1}	UNCALIBRATED [CALIBRATE]: 35 000.
T_{ref}	Arrhenius reference temperature	K	FIXED: 298.15 (25 °C). Reference point only, not a rate.
n	Saturation-factor exponent	dimensionless	ASSUMED: 2/3 (shrinking core).
w^*	Optimal solid moisture (set-point)	kg kg^{-1}	UNCALIBRATED [CALIBRATE]: 0.17.
σ_w	Width of the moisture optimum	kg kg^{-1}	UNCALIBRATED [CALIBRATE]: 0.08.
ΔH_R	Heat of reaction (exothermic)	J mol^{-1} CO_2	LITERATURE: −114 700 (liquid product water; latent heat is treated separately, net ≈ −70.7 kJ mol^{-1}, ≈ 83 W at EN 14143).
k_e	Solid–gas moisture exchange coefficient	s^{-1}	UNCALIBRATED [CALIBRATE]: 1.5×10^{-3}.

Table A2. Thermal and transport parameters.

Symbol	Meaning	Unit	How the value was defined (notes)
$C_{p,g}$	Loop-gas molar heat capacity	J mol^{-1} K^{-1}	LITERATURE: 29.1 (N_2/O_2/He mix).
$C_{p,s}$	Absorbent specific heat capacity	J kg^{-1} K^{-1}	UNCALIBRATED [CALIBRATE]: 900.
h_v	Interphase (gas–solid) heat-transfer coefficient	W m^{-3} K^{-1}	UNCALIBRATED [CALIBRATE]: 2×10^4.
h_w	Wall heat-transfer coefficient	W m^{-2} K^{-1}	UNCALIBRATED [CALIBRATE]: 200 (with $r = 0.25$). Only the product $(1-r)h_w$ is identifiable.
r	Jacket recovery factor	dimensionless, [0, 1]	BOUNDED by the energy balance (Sections 4.5 and 12.4) to ~0.1–0.3; default 0.25. $r = 0$ is a bare wall. With $h_w = 200$ W m^{-2} K^{-1}, $(1-r)h_w = 150$ W m^{-2} K^{-1}.
α_g	Effective gas thermal diffusivity	m^2 s^{-1}	UNCALIBRATED [CALIBRATE]: 0.03. Lumps conduction and mixing. Not used in the implementation (quasi-steady gas).
α_s	Effective solid thermal diffusivity	m^2 s^{-1}	UNCALIBRATED [CALIBRATE]: 2×10^{-5}. The implementation uses the equivalent bed conductivity 1.5 W m^{-1} K^{-1} ($\alpha_s \approx 2 \times 10^{-6}$ m^2 s^{-1}).

Symbol	Meaning	Unit	How the value was defined (notes)
D	Axial dispersion coefficient	$m^2\ s^{-1}$	UNCALIBRATED [CALIBRATE]: 1×10^{-4}. Confounded with numerical diffusion (Section 10). Not used in the implementation.
ρ_s	Solid-phase (granule) density	$kg\ m^{-3}$	DERIVED, Eq. (10): $\rho_s = m/\left((1-\varepsilon)V_{bed}\right) \approx 1435$. Never set by hand; fixed by the charge.

Table A3. Parameters of the stochastic formulation and its implementation. Values are those used for the results of Section 12.

Symbol	Meaning	Unit	How the value was defined (notes)
M	Reactive domains per cell	count	USER-SET: 50. The mean is insensitive to M for $M \geq 10$; the run-to-run spread decreases as M increases.
Δt	Time step of the solid update and of event sampling	s	USER-SET: 5 (Section 10).
$d_{p,0}$, σ_d	Reference grain size; log-standard deviation of domain grain size	m; —	$d_{p,0}$ = 3 mm cancels in (9e) and is documentation only; σ_d = 0.25 (lognormal).
k_{init}	Initiation coefficient	$m^3\ mol^{-1}\ s^{-1}$	UNCALIBRATED [CALIBRATE]: 2.0.
h_0, b	Passivation hazard coefficient; conversion exponent	—	UNCALIBRATED [CALIBRATE]: h_0 = 3.0, b = 2. Set the stranded capacity.
a_w	Moisture-stress weight of the passivation hazard	—	UNCALIBRATED [CALIBRATE]: 0.5.
w_{init}	Initial mean moisture	$kg\ kg^{-1}$	USER-SET: 0.17.
σ_{batch}, σ_{node}, σ_{dom}	Run-level, path-correlated and domain-level standard deviations of the initial moisture	$kg\ kg^{-1}$	0.01; 0.015 (first-order autoregressive, correlation 0.8 between neighboring cells); 0.03.
σ_χ	Log-standard deviation of the hygroscopicity factor $\chi_{i,j}$ (mean 1)	—	0.20.
$w_{eq,max}$, w_{max}	Equilibrium moisture at $RH = 1$; maximum moisture held	$kg\ kg^{-1}$	UNCALIBRATED [CALIBRATE]: 0.20; 0.40 (excess drains).
ψ	Pressure exponent of the rate constant	—	UNCALIBRATED [CALIBRATE]: 0.5 (0 reaction-limited, 1 film-diffusion-limited).
L_v	Latent heat of vaporization of water	$J\ mol^{-1}$	LITERATURE: 44 000.
—	Fraction of $T_b - T_\infty$ retained by the gas at the canister inlet	—	FIXED: 0.5.
—	Initial bed temperature	°C	USER-SET: 20.
—	Monte Carlo runs per canister	count	USER-SET: 40 (seeds 1–40 and 100001–100040).